

# Learning Heterogeneous Performance-Fairness Trade-offs in Federated Learning

Rongguang Ye, Ming Tang\*

Department of Computer Science and Engineering and the Research Institute of Trustworthy Autonomous Systems at Southern University of Science and Technology, Shenzhen, China.  
yerg2023@mail.sustech.edu.cn, tangm3@sustech.edu.cn

## Abstract

Recent methods leverage a hypernet to handle the performance-fairness trade-offs in federated learning. This hypernet maps the clients' preferences between model performance and fairness to preference-specific models on the trade-off curve, known as local Pareto front. However, existing methods typically adopt a uniform preference sampling distribution to train the hypernet across clients, neglecting the inherent heterogeneity of their local Pareto fronts. Meanwhile, from the perspective of generalization, they do not consider the gap between local and global Pareto fronts on the global dataset. To address these limitations, we propose HetPFL to effectively learn both local and global Pareto fronts. HetPFL comprises Preference Sampling Adaptation (PSA) and Preference-aware Hypernet Fusion (PHF). PSA adaptively determines the optimal preference sampling distribution for each client to accommodate heterogeneous local Pareto fronts. While PHF performs preference-aware fusion of clients' hypernets to ensure the performance of the global Pareto front. We prove that HetPFL converges linearly with respect to the number of rounds, under weaker assumptions than existing methods. Extensive experiments on four datasets show that HetPFL significantly outperforms seven baselines in terms of the quality of learned local and global Pareto fronts.

## 1 Introduction

Federated Learning (FL) [McMahan *et al.*, 2017] is an emerging machine learning paradigm that designed to train neural network models using data silos while preserving data privacy. In recent years, FL has achieved remarkable success across various domains, including healthcare [Rieke *et al.*, 2020], fintech [Imteaj and Amini, 2022], and the Internet of Things (IoT) [Nguyen *et al.*, 2021]. As FL continues to develop, the issue of group fairness has become an increasingly significant focus. Specifically, there are two primary types of group fairness in FL: client-based fairness [Li *et al.*, 2019;

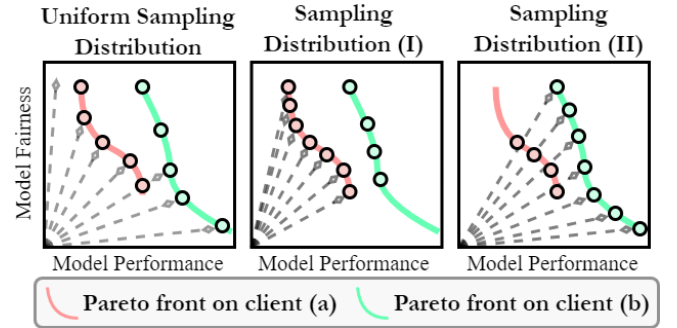


Figure 1: The impact of different sampling distributions under two clients. The dotted vectors represent preferences for model's performance and fairness. The pink and green points are loss vectors of the model after evaluation on the local dataset on client (a) and client (b), respectively. A uniform preference sampling distribution cannot achieve the best result of learning local Pareto fronts based on Lemma 1. Instead, sampling distribution (I) is suitable for client (a), and sampling distribution (II) is suitable for client (b).

Lyu *et al.*, 2020; Wang *et al.*, 2021] and group-based fairness [Yue *et al.*, 2023; Deng *et al.*, 2020]. Client-based fairness aims to minimize the variance in model performance across clients while preserving the overall model performance. Our work focuses on group-based fairness, which ensures that a model performs equitably across different demographic subgroups (e.g., male or female) within each local dataset [Kamishima *et al.*, 2012; Roh *et al.*, 2020].

Recent studies have focused on improving the group-based fairness of FL by proposing data sampling strategies and designing new optimization objectives. In terms of data sampling strategies, FedFB [Zeng *et al.*, 2021] adjusts the sampling probabilities of subgroup samples during training, increasing the probability of underperforming groups to achieve group fairness. Meanwhile, FairFed [Ezzeldin *et al.*, 2023] adopts a fairness-aware model aggregation scheme. Regarding the design of optimization objectives, LFT+FedAvg [Zeng *et al.*, 2023] incorporates group fairness as a constraint during local training. FAIR-FATE [Salazar *et al.*, 2023] introduces a linear combination of model performance and group fairness as its objective function. In fact, a trade-off exists between model per-

\*Corresponding Author.

formance and model fairness, meaning that improving fairness often comes at the cost of performance. With respect to efficiency, learning the entire performance-fairness trade-off curve (i.e., the Pareto front) for each client offers a more flexible scheme. Moreover, in terms of generalization, it is crucial to consider the quality of the global Pareto front on the global dataset. Recent studies [Lin *et al.*, 2022; Ye *et al.*, 2025] have introduced hypernets to learn the local Pareto front on the local dataset by modeling the mapping from a predefined preference distribution to preference-specific models. However, these methods still exhibit limitations in efficiency and generalization within the FL context:

- **Efficiency:** As shown in Fig. 1, the heterogeneity of data in FL results in differences in the positions of local Pareto fronts across clients. Each local Pareto front has its own optimal preference sampling distribution. However, prior approaches assume a uniform preference sampling distribution across clients, which is inefficient for learning local Pareto fronts.
- **Generalization:** Achieving both optimal local and global Pareto fronts presents inherent conflicts. Prior approaches primarily focus on improving the local Pareto front while neglecting the global Pareto front.

Addressing these limitations presents several challenges. In terms of efficiency, determining the optimal preference sampling distribution for each client is non-trivial, as the position of each client’s local Pareto front (ground truth) is initially unknown. Regarding generalization, aggregating clients’ models to construct the optimal global model is difficult, as it requires identifying the strengths of each client’s model for different preferences while maintaining data privacy.

In this paper, we propose HetPFL to efficiently learn both local and global Pareto fronts. HetPFL consists of Preference Sampling Adaptation (PSA) and Preference-aware Hypernet Fusion (PHF). PSA dynamically adjusts the preference sampling distribution by introducing data-driven HyperVolume Contribution (HVC), which quantifies each preference’s contribution to the learned Pareto front. We then jointly optimize the preference sampling distribution based on HVC and the client’s model as a bi-level optimization problem to enhance local Pareto front learning efficiency. To improve the global Pareto front, PHF considers a preference-aware hypernet aggregation at the server by identifying the capability of each client’s hypernet for various preferences.

The primary contributions of this work are as follows:

- We propose a HetPFL framework that efficiently learns the heterogeneous local Pareto fronts across clients using PSA, while simultaneously achieving a high-quality global Pareto front through PHF;
- We analyze the convergence rate of HetPFL within the FL system and establish an error convergence rate of order  $\mathcal{O}(\frac{1}{t})$ . This result is particularly challenging to derive due to the interdependence of the different components in the FL system;
- Extensive experiments on four datasets demonstrate that HetPFL outperforms the best-performing baseline,

achieving approximately 1.75% and 5.5% improvements in the quality of the learned local and global Pareto fronts, respectively.

## 2 Problem Formulation

Let  $\mathbf{x} \in \mathcal{X}$ ,  $y \in \mathcal{Y}$  denote features and label, respectively. The features in  $\mathbf{x} \triangleq (\mathbf{a}, \mathbf{b})$  contain sensitive features  $\mathbf{a}$  (e.g., gender, race) and non-sensitive features  $\mathbf{b}$ . Suppose there are  $K$  clients, and each client  $k \in [K]$  has a local dataset, denoted by  $\mathcal{D}_k$ . The classifier  $f_{\theta_k}$  with learnable parameters  $\theta_k$  of client  $k$  outputs a prediction  $f_{\theta_k}(\mathbf{x})$  from an input data  $\mathbf{x}$ .

According to [Zeng *et al.*, 2021], we define loss functions for model performance and fairness, respectively. Usually, model performance is characterized using cross-entropy loss

$$\ell_{CE}(\mathbf{x}, y | f_{\theta_k}) = -[y \log(f_{\theta_k}(\mathbf{x})) + (1 - y) \log(1 - f_{\theta_k}(\mathbf{x}))]. \quad (1)$$

We use following loss function to quantify model fairness:

$$\ell_F(\mathbf{x}, y | f_{\theta_k}) = [(\mathbf{a} - \bar{\mathbf{a}}_k)(f_{\theta_k}(\mathbf{x}) - \bar{f}_{\theta_k}(\mathbf{x}))], \quad (2)$$

where  $\bar{\mathbf{a}}_k$  and  $\bar{f}_{\theta_k}(\mathbf{x})$  represent the average values of  $\mathbf{a}$  and  $f_{\theta_k}(\mathbf{x})$  over  $\mathcal{D}_k$ , respectively.  $\ell_F$  measures the correlation between sensitive features and model predictions. When the model prediction exhibits a stronger correlation with sensitive features, the value of  $\ell_F$  rises, signaling a reduced model fairness.

The trade-off between  $\ell_{CE}$  and  $\ell_F$  is quantified using a preference vector  $\boldsymbol{\lambda} \in \Lambda = \{\boldsymbol{\lambda} \in \mathbb{R}_+^2 \mid \sum_{i=1}^2 \lambda_i = 1\}$ . Following [Ye *et al.*, 2025], we introduce a hypernet  $h_{\beta_k} : \mathbb{R}^{|\boldsymbol{\lambda}|} \rightarrow \mathbb{R}^{|\theta_k|}$  with learnable parameters  $\beta_k$ , which maps a preference vector  $\boldsymbol{\lambda}$  to a preference-specific model  $\theta_k = h_{\beta_k}(\boldsymbol{\lambda})$ . We aim at optimizing  $\beta_k$  to improve model performance and fairness (i.e., reducing the losses in Eqs. (1) and (2)), for which we can define a *weighted Tchebycheff scalar* loss [Miettinen, 1999] for each preference vector  $\boldsymbol{\lambda}$ :

$$\min_{\beta_k} g_{\text{tch}}(\mathbf{x}, y, h_{\beta_k}(\boldsymbol{\lambda}) | \boldsymbol{\lambda}) = \max_{j \in \{CE, F\}} \left\{ \frac{\ell_j(\mathbf{x}, y | h_{\beta_k}(\boldsymbol{\lambda}))}{\lambda_j} \right\}. \quad (3)$$

Eq. (3) satisfies the following Lemma [Miettinen, 1999]:

**Lemma 1** (Preference Alignment). *Given a preference vector  $\boldsymbol{\lambda}$ , a preference-specific model  $h_{\beta_k}(\boldsymbol{\lambda})$  is weakly Pareto optimal to the problem (3) if and only if  $h_{\beta_k}(\boldsymbol{\lambda})$  is optimal for problem (3).*

We give a schematic diagram of weakly Pareto optimality and Pareto optimality in Fig. 6 of the Appendix. Lemma 1 guarantees that when  $h_{\beta_k}(\boldsymbol{\lambda})$  is optimal for problem (3), the loss vector  $(\ell_{CE}, \ell_F)$  of  $h_{\beta_k}(\boldsymbol{\lambda})$  on dataset  $\mathcal{D}_k$  aligns exactly with the direction of the preference vector and lies on the Pareto front, as shown by the points in Fig. 1.

We consider optimizing Eq. (3) over the preference distribution  $\Lambda_k$  of each client  $k$ , and define the following goal for the **local Pareto front** learning of client  $k$ .

$$\min_{\beta_k} \mathbb{E}_{\boldsymbol{\lambda} \sim \Lambda_k} \mathbb{E}_{(\mathbf{x}, y) \in \mathcal{D}_k} g_{\text{tch}}(\mathbf{x}, y, h_{\beta_k}(\boldsymbol{\lambda}) | \boldsymbol{\lambda}), \quad (4)$$

where  $\Lambda_k$  is unknown in advance and depends on the position of the Pareto front of client  $k$ . Preference vector  $\boldsymbol{\lambda}$  is sampled from  $\Lambda_k$ . Once Eq. (4) is completed, the hypernet can receive all possible preference vectors as inputs,

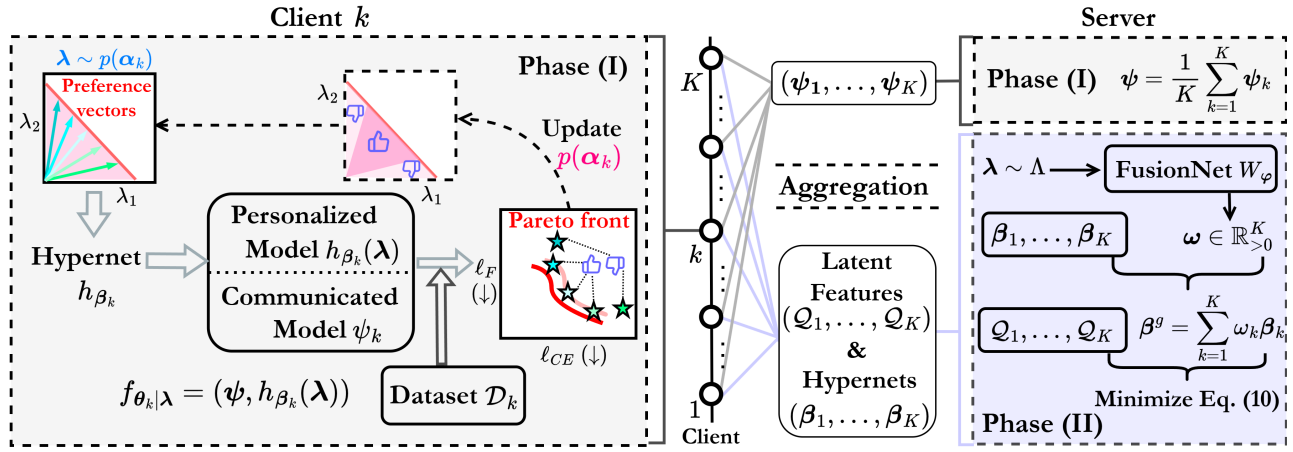


Figure 2: HetPFL framework.

generating a corresponding set of preference-specific models  $\{\theta_k = h_{\beta_k}(\lambda) \mid \lambda \sim \Lambda_m\}$ . This model set is then evaluated on the local dataset  $\mathcal{D}_k$ , and the evaluation results collectively form the entire local Pareto front.

Similarly, the goal for the **global Pareto front** is to generate an aggregated hypernet  $\beta^g = \frac{1}{K} \sum_{k=1}^K \beta_k$ , which minimizes the  $g_{\text{tch}}(\cdot)$  over the global dataset:

$$\min_{\beta^g} \frac{1}{K} \sum_{k=1}^K \mathbb{E}_{\lambda \sim \Lambda} \mathbb{E}_{(x,y) \in \mathcal{D}_k} g_{\text{tch}}(x, y, h_{\beta^g}(\lambda) \mid \lambda), \quad (5)$$

where  $\Lambda$  can be an arbitrary distribution or defined as a combination of  $\Lambda_1, \dots, \Lambda_K$ .

Our goal is to optimize Eq. (4) for all clients while simultaneously optimizing Eq. (5). The primary challenge in Eq. (4) arises from the distinctiveness of each client's local Pareto front. This implies the necessity of approximating preference distribution  $\Lambda_k$  for each client  $k$  to effectively learn the local Pareto fronts. For Eq. (5), the optimization objectives for local and global Pareto fronts are inherently conflicting, preventing simultaneous optimality for both.

### 3 Methodology

This section presents our HetPFL framework. We provide an overview and introduce the two main components, PSA and PHF, of HetPFL in Sections 3.1–3.3. Sections 3.4–3.5 describe the optimization procedure of HetPFL and analyze its convergence properties.

#### 3.1 Overview

Fig. 2 shows our proposed HetPFL. The foundational components of HetPFL include communicated model  $\psi$ , hypernet  $h_{\beta_k}$ , preference sampling distribution  $p(\alpha_k)$ , and FusionNet  $W_\varphi$ . HetPFL can be divided into two phases. Phase (I) focuses on efficiently learning the local Pareto fronts for all clients, while Phase (II) aims to learn the global Pareto front.

##### Phase (I)

In this phase, we aim to optimize the hypernet, sampling distribution, and the communicated model. The communicated model  $\psi$  transforms the features into  $d$ -dimensional latent

features and is periodically aggregated at the server, as in FL. The hypernet  $h_{\beta_k}$  is kept locally at the client in Phase (I). Its role is to map an arbitrary preference vector  $\lambda$  into a preference-specific model  $h_{\beta_k}(\lambda)$ , and then  $h_{\beta_k}(\lambda)$  transforms the  $d$ -dimensional latent features to label. For each client  $k$ , we denote  $f_{\theta_k|\lambda} = (\psi, h_{\beta_k}(\lambda))$ .

Previous works simply set preference sampling distribution  $p(\alpha_k)$  to be uniform across all clients. In contrast, we consider jointly optimizing the hypernet  $h_{\beta_k}$  and  $p(\alpha_k)$ :

$$\min_{\beta_k, \alpha_k} \mathbb{E}_{\lambda \sim p(\alpha_k)} \mathbb{E}_{(x,y) \in \mathcal{D}_k} g_{\text{tch}}(x, y, f_{\theta_k|\lambda}), \quad (6)$$

where  $\alpha_k$  are the parameters of  $p(\alpha_k)$ . HetPFL improves the efficiency of learning local Pareto fronts by identifying a suitable  $p(\alpha_k)$  for each client over the preference space. Meanwhile, the communicated model optimized to improve the model performance of all clients:

$$\min_{\psi} \frac{1}{K} \sum_{k=1}^K \mathbb{E}_{(x,y) \in \mathcal{D}_k} [\ell_{CE}(x, y, f_{\theta_k|\tilde{\lambda}})], \quad (7)$$

where  $f_{\theta_k|\tilde{\lambda}} = (\psi, h_{\beta_k}(\tilde{\lambda}))$  and  $\tilde{\lambda}$  is a predefined preference vector. The details of update steps for Eqs. (6) and (7) are provided in Section 3.4.

##### Phase (II)

Unlike previous works that overlook the global Pareto front, Phase (II) focuses on addressing this gap. After the final round, clients first transmit their hypernets and latent features,  $Q_k = \psi(x) \mid (x, y) \in \mathcal{D}_k$ , to the server. The server then uses FusionNet,  $W_\varphi$ , with parameters  $\varphi$  to learn effective aggregation strategies for these hypernets, tailoring the aggregation process to different preference vectors. Notably, transmitting only the latent features of the dataset is a common practice to mitigate privacy concerns [Thapa *et al.*, 2022].

Given this framework, two key questions remain to be addressed. First, how can  $p(\alpha_k)$  be determined in Phase (I) to enable efficient learning of local Pareto fronts? Second, how to optimize FusionNet in Phase (II)? These questions will be explored in the following two subsections.

### 3.2 Preference Sampling Adaptation

In Phase (I), we propose Preference Sampling Adaptation (PSA) to determine  $p(\alpha_k)$ . Determining  $p(\alpha_k)$  involves optimizing the quality of the sampled preference vectors during training. This process is non-trivial and unfolds in two steps: first, evaluating the quality of the sampled preference vectors without a true Pareto front (ground truth); and second, integrating the optimization of  $p(\alpha_k)$  into the hypernet’s training.

For the first step, we introduce a data-driven Hypervolume Contribution (HVC) indicator to assess the quality of sampled preference vectors. Despite the absence of a true local Pareto front, it allows for quantifying each preference vector’s contribution based on the training losses.

**Definition 1 (HVC).** Given a reference point  $\mathbf{r}$ . Let  $\mathcal{S}(\lambda, \mathbf{r}) = \{\mathbf{q} \in \mathbb{R}^2 \mid \ell(\mathbf{x}, \mathbf{y} \mid f_{\theta_k|\lambda}) \leq \mathbf{q} \text{ and } \mathbf{q} \leq \mathbf{r}\}$ , and the hypervolume of a set of  $N$  preference vectors  $\Lambda_{\alpha_k} = \{\lambda^1, \dots, \lambda^N \mid \lambda^i \sim p(\alpha_k)\}$  is

$$\mathcal{H}_{\mathbf{r}}(\Lambda_{\alpha_k}) = \mathcal{L}\left(\bigcup_{\lambda \in \Lambda_{\alpha_k}} \mathcal{S}(\lambda, \mathbf{r})\right),$$

where  $\mathcal{L}(\cdot)$  denotes the Lebesgue measure and  $\mathbf{q}$  represents any point in the gray area in the left figure of Fig. 3. The HVC of  $f_{\theta_k|\lambda^i}$  for the set  $\Lambda_{\alpha_k}$  is the difference between  $\mathcal{H}_{\mathbf{r}}(\Lambda_{\alpha_k})$  and  $\mathcal{H}_{\mathbf{r}}(\Lambda_{\alpha_k} \setminus \lambda^i)$ , as follows:

$$\mathcal{HC}_{\mathbf{r}}(\lambda^i \mid \Lambda_{\alpha_k}) = \mathcal{H}_{\mathbf{r}}(\Lambda_{\alpha_k}) - \mathcal{H}_{\mathbf{r}}(\Lambda_{\alpha_k} \setminus \lambda^i).$$

Fig. 3 shows that the HVC of  $f_{\theta_k|\lambda^i}$  is the difference between the HV of the full set of five models and that of the set excluding  $f_{\theta_k|\lambda^i}$ . The larger  $\mathcal{HC}_{\mathbf{r}}(\lambda^i \mid \Lambda_{\alpha_k})$ , the greater the contribution of  $\lambda^i$ , indicating a higher quality of  $\lambda^i$ .

We then move on to the second step. Based on HVC, we propose the following bi-level optimization objective to alternately optimize the hypernet and the preference sampling distribution of client  $k$ :

$$\min_{\alpha_k} \mathbb{E}_{\lambda \sim p(\alpha_k)} \mathbb{E}_{(\mathbf{x}, \mathbf{y}) \in \mathcal{D}_k} [-\mathcal{HC}_{\mathbf{r}}(\lambda \mid \Lambda_{\alpha_k})], \quad (8)$$

$$\text{s.t. } \beta_k = \arg \min_{\beta_k} \mathbb{E}_{\lambda \sim p(\alpha_k)} \mathbb{E}_{(\mathbf{x}, \mathbf{y}) \in \mathcal{D}_k} [g_{\text{tch}}(\mathbf{x}, \mathbf{y}, f_{\theta_k|\lambda})], \quad (9)$$

where  $f_{\theta_k|\lambda} = (\psi_k, h_{\beta_k}(\lambda))$ . The bi-level optimization first optimizes the hypernet as in Eq. (9). Then, the sampling distribution is further refined based on the solution of Eq. (9). As shown in Fig. 2, it makes the sampling distribution at the next iteration more beneficial to local Pareto front learning.

### 3.3 Preference-aware Hypernet Fusion

In Phase (II), we propose a preference-aware hypernet fusion (PHF) method. The intuition behind PHF is that each client’s hypernet excels at specific preference vectors. Thus, for any given preference vector, PHF learns the preference-aware aggregation weight so that hypernets specializing in that vector are given higher weight, thereby improving the quality of the global Pareto front. As shown in Fig. 2, we introduce a FusionNet  $W_{\varphi} : \mathbb{R}^{|\lambda|} \rightarrow \mathbb{R}_{\geq 0}^K$  with parameters  $\varphi$  that learns a mapping from any preference vector  $\lambda$  to a fusion weight  $\omega = W_{\varphi}(\lambda) \in \mathbb{R}^K$ . Based on the fusion weight, the hypernets from all clients are linearly combined to form a global

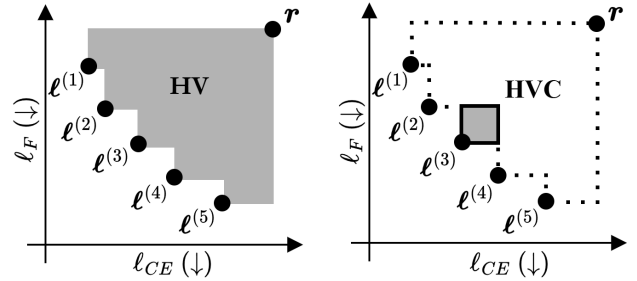


Figure 3: An illustration of the HV and HVC of the loss vectors  $\ell^{(i)}$  produced by evaluating a model set  $\{f_{\theta_k|\lambda^i}\}_{i=1}^5$  corresponding to five input preference vectors.

hypernet  $\beta^g = W_{\varphi}(\lambda) \cdot [\beta_1, \dots, \beta_K]$ , where operation  $\cdot$  is the vector inner product. This process is optimized through

$$\min_{\varphi} \mathbb{E}_{\lambda \sim \Lambda} \left[ \frac{1}{K} \sum_{k=1}^K g_{\text{tch}}(\mathcal{Q}_k, \mathcal{Y}_k, f_{\theta_k^g|\lambda}) \right], \quad (10)$$

where  $f_{\theta_k^g|\lambda} = (\psi, h_{\beta^g}(\lambda))$ , and  $\mathcal{Y}_k$  represents labels on dataset  $\mathcal{D}_k$ . Recalling Lemma 1, the global hypernet  $f_{\theta_k^g|\lambda}$  aggregated by FusionNet is optimized towards the direction where the Pareto front intersects with  $\lambda$ . Once Eq. (10) is solved, the mapping from preference vectors to fusion weights during inference is highly efficient.

### 3.4 Algorithm: HetPFL

In this subsection, we present HetPFL algorithm to optimizing four components including communicated model  $\psi$ , hypernet  $h_{\beta_k}$ , preference sampling distribution  $p(\alpha_k)$ , and FusionNet  $W_{\varphi}$ . At the beginning of Phase (I), each client downloads the global communicated model  $\theta_k^0$  from the server.

In round  $t$ , the communicated model on client  $k$  is updated through  $\tau_c$  steps of gradient descent with a learning rate of  $\eta_t$ :

$$\psi^t \leftarrow \psi^t - \eta_t \mathbb{E}_{(\mathbf{x}, \mathbf{y}) \in \mathcal{D}_k} \nabla_{\psi} [\ell_{CE}(\mathbf{x}, \mathbf{y} \mid f_{\theta_k|\tilde{\lambda}})]. \quad (11)$$

To balance model performance and fairness, we set  $\tilde{\lambda}$  to  $(\frac{1}{2}, \frac{1}{2})$  in Eq. (11). Then, we proceed to optimize the hypernet and the preference sampling distribution (in Eqs. (9) and (8)). Note that lower-level problem (Eq. (9)) is a stochastic optimization problem, which is challenging to solve directly due to the expectation over preference distribution involving infinite possible values. To address this, we approximate the expectation term using Monte Carlo sampling and then solve the Eq. (9) with  $\tau_p$  steps of gradient descent

$$\beta_k^t \leftarrow \beta_k^t - \frac{\eta_t}{N} \mathbb{E}_{(\mathbf{x}, \mathbf{y}) \in \mathcal{D}_k} \sum_{v=1}^N \nabla_{\beta_k} g_{\text{tch}}(\mathbf{x}, \mathbf{y}, f_{\theta_k|\lambda^v} \mid \lambda^v), \quad (12)$$

where  $\eta_t$  denotes the learning rate,  $\lambda^v$  is a sampled preference vector and  $N$  is the number of sampled preference vectors.

Solving the upper-level problem in Eq. (8) relies on computing the HVC gradient, given by  $g_{\alpha_k} = \nabla_{\alpha_k} \mathbb{E}_{\lambda \in \Lambda_{\alpha_k}} \mathbb{E}_{(\mathbf{x}, \mathbf{y}) \in \mathcal{D}_k} [-\mathcal{HC}_{\mathbf{r}}(\lambda \mid \Lambda_{\alpha_k})]$ . However, since this gradient is sometimes non-differentiable, we employ

Natural Evolution Strategies (NES) [Salimans *et al.*, 2017], which yield gradient estimation  $\hat{g}_{\alpha_k}$  for  $g_{\alpha_k}$ :

$$\hat{g}_{\alpha_k} \approx \mathbb{E}_{\lambda \in \Lambda_{\alpha_k}} [-\mathcal{H}C_r(\lambda | \Lambda_{\alpha_k}) \nabla_{\alpha_k} \log p(\lambda | \alpha_k)], \quad (13)$$

where  $\Lambda_{\alpha_k}$  is the set of  $N$  preference vectors collected in Eq. (12). This gradient computation method only requires the preference sampling distribution  $p(\alpha_k)$  to be differentiable, without the need for HVC function to be differentiable. Based on Eq. (13), to optimize Eq. (8),  $\alpha_k$  is updated using the gradient  $\hat{g}_{\alpha}$  by performing  $\tau_p$  steps of gradient descent:

$$\alpha_k^t \leftarrow \alpha_k^t - \kappa_t \hat{g}_{\alpha_k}, \quad (14)$$

where  $\kappa_t$  is the learning rate. After round  $t$  is completed, all clients transmit their communicated models  $\psi_k, k \in [K]$ , to the server. The server updates the communicated model by performing an averaging aggregation

$$\psi_k^{t+1} = \frac{1}{K} \sum_{k=1}^K \psi_k^t. \quad (15)$$

Subsequently, each client initializes the communicated model as the aggregated model for round  $t+1$ .

Upon completing a total of  $T$  rounds, we proceed to Phase (II), where the optimization of  $\varphi^t$  is updated by

$$\varphi^t \leftarrow \varphi^t - \eta_t \frac{1}{N} \frac{1}{K} \sum_{v=1}^N \sum_{k=1}^K \nabla_{\varphi} g_{\text{tch}}(\mathcal{Q}_k, \mathcal{Y}, f_{\theta_k^q | \lambda} | \lambda), \quad (16)$$

where  $\eta_t$  is the learning rate. We provide the pseudocode of the HetPFL algorithm in the Appendix.

### 3.5 Theoretical Analysis

In this subsection, we theoretically analyze the convergence of HetPFL algorithm. Our proof process is structured in two main steps. Firstly, we establish an upper bound of the communicated model at any given round  $t$ . Next, we provide the upper bound of the hypernet at any given round  $t$ .

To simplify the notation, we represent the expressions of Eqs. (8) and (9) as  $g_{\text{hvc}}(\alpha_k, \beta_k) = \mathbb{E}_{\lambda \sim p(\alpha_k)} \mathbb{E}_{(x,y) \in \mathcal{D}_k} [-\text{HVC}_r(\lambda | \Lambda_{\alpha_k})]$  and  $g_{\text{tch}}(\alpha_k, \beta_k) = \mathbb{E}_{\lambda \sim p(\alpha_k)} \mathbb{E}_{(x,y) \in \mathcal{D}_k} [g_{\text{tch}}(x, y, f_{\theta_k | \lambda} | \lambda)]$ , respectively.

Based on [Hong *et al.*, 2023], we make the following assumptions.

**Assumption 1.**  $\nabla_{\beta} g_{\text{tch}}(\alpha_k, \beta_k)$ ,  $\nabla_{\alpha\beta}^2 g_{\text{tch}}(\alpha_k, \beta_k)$ ,  $\nabla_{\beta\beta}^2 g_{\text{tch}}(\alpha_k, \beta_k)$ ,  $\nabla_{\alpha} g_{\text{hvc}}(\alpha_k, \beta_k)$ , and  $\nabla_{\beta} g_{\text{hvc}}(\alpha_k, \beta_k)$  are Lipschitz continuous in  $\beta_k$  with respective Lipschitz constants  $L_{t1}$ ,  $L_{t2}$ ,  $L_{t3}$ ,  $L_{h1}$  and  $L_{h2}$ .

**Assumption 2.**  $\nabla_{\alpha\beta}^2 g_{\text{tch}}(\alpha_k, \beta_k)$ ,  $\nabla_{\beta\beta}^2 g_{\text{tch}}(\alpha_k, \beta_k)$ ,  $\nabla_{\beta} g_{\text{hvc}}(\alpha_k, \beta_k)$  is Lipschitz continuous in  $\alpha_k$  with respective Lipschitz constants  $L_{t4}$ ,  $L_{t5}$  and  $L_{h3}$ .

**Assumption 3.**  $g_{\text{tch}}(\alpha_k, \beta_k)$  is  $\mu_1$ -strongly convex in  $\beta_k$ , and  $g_{\text{tch}}(\beta_k, \alpha_k^*)$  is  $\mu_2$ -strongly convex in  $\beta_k$ , where  $\alpha_k^*$  is optimal sampling distribution for client  $k$ .

**Assumption 4.** The expectation of stochastic gradients is always bounded. That is,  $\|\nabla_{\alpha\beta}^2 g_{\text{tch}}(\alpha_k, \beta_k)\| \leq G_1$ ,  $\|\nabla_{\alpha} g_{\text{hvc}}(\alpha_k, \beta_k)\| \leq G_2$ , and  $\|\nabla_{\beta} g_{\text{tch}}(\alpha_k, \beta_k)\| \leq G_3$ .

Let  $\Delta_{\beta_k}^t \triangleq \mathbb{E} [\|\beta_k^t - \beta_k^* | \alpha_k^{t-1}\|^2]$  denote the error between the hypernet at round  $t$  and the optimal hypernet  $\beta_k^* | \alpha_k^{t-1}$  given the sampling distribution  $p(\alpha_k^{t-1})$  in round  $t-1$ . Let  $\Delta_{\psi_k}^t \triangleq \mathbb{E} [\|\psi_k^t - \psi_k^*\|^2]$  denote the error between the communicated model at round  $t$  and the optimal communicated model  $\psi_k^*$ . The communicated model has following upper bound.

**Lemma 2** (Convergence of the Communicated Model [Collins *et al.*, 2021]). *If the communicated model  $\psi$  is optimized by FedAvg [McMahan *et al.*, 2017] and given a constant  $\zeta > 0$ , then  $\psi$  converges to the optimal communicated model  $\psi^*$  at a linear rate:*

$$\Delta_{\psi_k}^t \leq (1 - \eta\zeta)^{t/2} \Delta_{\psi_k}^0, \quad (17)$$

with a probability at least  $1 - te^{-100 \min(|x|^2 \log(|K|), d)}$ .

Lemma 2 shows that the error convergence rate is  $\mathcal{O}(\frac{1}{t})$ . Under weaker assumptions compared to [Ye *et al.*, 2025] (i.e., without requiring the initial convergence error of the hypernet to be a constant multiple of the communicated model), we establish the following upper bound for hypernet. The detailed proof can be found in the Appendix.

**Theorem 1** (Convergence of the Hypernet). *Under Assumptions 1-4 and Lemma 2, the upper bound of hypernet is*

$$\begin{aligned} \Delta_{\beta_k}^{t+1} \leq & \left(\frac{3}{4}\right)^{\tau_p t} \Delta_{\beta_k}^0 + z_1 (1 - \eta_t \zeta)^{t/4} \sqrt{\Delta_{\psi_k}^0} \\ & + z_2 (1 - \eta_t \zeta)^{t/2} \Delta_{\psi_k}^0 + \frac{\sigma_1^2 \mu_1 + c_1^2 L_{q1}^2 + G_3^2 \mu_1}{\mu_1^3} \\ & + 2\eta_t L_{t1} (1 - \eta_t \zeta)^{t/4} \sqrt{\Delta_{\psi_k}^0 \Delta_{\beta_k}^0}, \end{aligned} \quad (18)$$

where  $z_1, z_2$  are constants, and  $\Delta_{\alpha_0}^t = \mathbb{E} [\|\alpha_k^0 - \alpha_k^*\|^2]$ . Theorem 1 guarantees an optimization error of order  $\mathcal{O}(\left(\frac{3}{4}\right)^{\tau_p t} + (1 - \eta_t \zeta)^{t/4} + (1 - \eta_t \zeta)^{t/2} + \frac{\sigma_1^2 \mu_1 + c_1^2 L_{q1}^2 + G_3^2 \mu_1}{\mu_1^3})$ .

When  $t \rightarrow +\infty$ ,  $\Delta_{\beta_k}^{t+1}$  converges to  $\frac{\sigma_1^2 \mu_1 + c_1^2 L_{q1}^2 + G_3^2 \mu_1}{\mu_1^3}$ . Due to  $(1 - \eta_t \zeta)^{t/4}$  being the dominant term in the error convergence rate, the overall error convergence rate is  $\mathcal{O}(\frac{1}{t})$ .

## 4 Experiments

### 4.1 Experimental Settings

**Datasets.** Four widely-used datasets are employed to evaluate the performance of HetPFL, including a SYNTHETIC [Zeng *et al.*, 2021], COMPAS [Barenstein, 2019], BANK [Moro *et al.*, 2014], and ADULT [Dua *et al.*, 2017].

**Baselines.** We compare HetPFL with seven state-of-the-art methods, including two for addressing local fairness (LFT+Ensemble and LFT+Fedavg [Zeng *et al.*, 2023]), three for global fairness (Agnosticfair [Du *et al.*, 2021], FairFed [Ezzeldin *et al.*, 2023] and FedFB [Zeng *et al.*, 2021]), one for both local and global fairness (Makhija *et al.*, 2024), and one for learning performance-fairness local Pareto fronts (PraFFL [Ye *et al.*, 2025]). PraFFL is the most closely related work to ours in learning Pareto fronts.

**Metrics.** Based on [Ezzeldin *et al.*, 2023], we use the model's error rate to quantify its performance and the DP disparity [Feldman *et al.*, 2015] to measure its fairness, where a

Table 1: Averaged performance comparison of different methods across four datasets over three runs. The best results are highlighted in bold, while the second-best results are underlined.

Method	SYNTHETIC		COMPAS		BANK		ADULT	
	Local HV	Global HV	Local HV	Global HV	Local HV	Global HV	Local HV	Global HV
LFT+Ensemble	0.425	0.479	0.514	0.555	0.890	0.881	0.760	0.764
LFT+Fedavg	0.700	0.468	0.505	0.514	0.891	0.138	0.765	0.501
Agnosticfair	0.492	0.537	0.499	0.550	0.887	0.880	<u>0.780</u>	<u>0.783</u>
FairFed	0.339	0.367	0.418	0.434	0.889	0.878	0.267	0.270
FedFB	0.567	0.608	0.505	0.517	0.893	0.883	0.759	0.763
EquiFL	0.642	0.604	0.564	0.526	0.892	0.882	0.761	0.764
PraFFL	<u>0.800</u>	<u>0.716</u>	<u>0.599</u>	<u>0.613</u>	<u>0.901</u>	<u>0.895</u>	0.766	0.750
HetPFL (Ours)	<b>0.830</b>	<b>0.827</b>	<b>0.623</b>	<b>0.626</b>	<b>0.904</b>	<b>0.898</b>	<b>0.783</b>	<b>0.846</b>

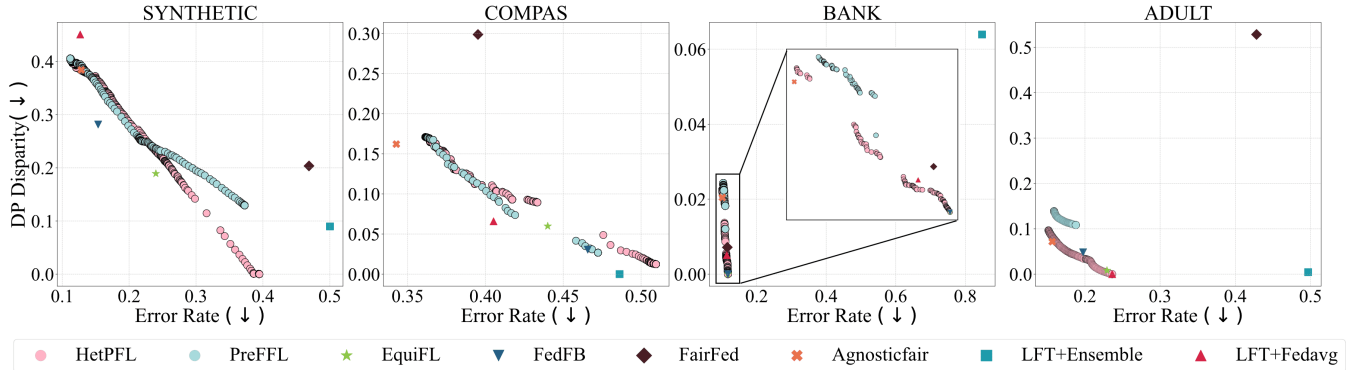


Figure 4: Comparison of global Pareto front obtained by our HetPFL algorithm and baselines on four datasets. A Pareto front closer to the bottom-left corner indicates better performance.

smaller DP disparity indicates a fairer model. Each point on the Pareto front represents a specific trade-off between performance and fairness in the two-dimensional objective space. Additionally, the hypervolume (HV) [Zitzler and Thiele, 1999] is employed to evaluate the quality of the learned Pareto front. We mainly report local HV on local datasets and global HV on global datasets in our experiments. **Hyperparameters.** Since PraFFL and HetPFL have the ability to generate any number of models during inference, we set them to generate 1,000 preference-specific models each for evaluation. See the Appendix for other detailed settings. Our implementation is available at <https://github.com/rG223/HetPFL>.

## 4.2 Experimental Results

We first present the main results and convergence analysis, followed by performance analysis across different scenarios, such as different levels of data heterogeneity and large-scale clients. Finally, an ablation study analyzing the two components of HetPFL is provided. **Main Results.** We draw two key conclusions based on Table 1: (I) Methods capable of learning the Pareto front, such as PraFFL and HetPFL, outperform those that do not in most cases, in terms of both local HV and global HV. Fig. 4 shows that PraFFL and HetPFL are capable of generating more models that caters to large-scale preferences; (II) PraFFL focuses primarily on learning local Pareto fronts, it neglects the heterogeneity of Pareto fronts across clients and fails to ensure the quality of

the global Pareto front, leading suboptimal on most datasets. In comparison, HetPFL outperforms PraFFL in terms of local HV and global HV across four datasets, achieving varying degrees of improvement. Fig. 4 indicates that HetPFL outperforms PraFFL on SYNTHETIC, BANK, and ADULT datasets. However, on the COMPAS, the Pareto front splits into two segments with a 3% disconnection in terms of DP disparity and error rate. HetPFL’s unimodal sampling distribution prioritizes the tail regions’ benefits while overlooking the middle sections compared to PraFFL.

**Convergence Results.** Fig. 5 shows the convergence comparison of PraFFL and HetPFL on the client local validation set in each round. HetPFL shows consistently faster convergence compared to the PraFFL, validating the effectiveness of our proposed preference sampling adaptation method.

**The Impact of Data Heterogeneity.** Table 2 demonstrates that HetPFL consistently achieves the best performance in both local HV and global HV across all levels of data heterogeneity compared to seven baselines. Notably, the following observations emerge: (I) **Comprehensiveness:** First five baselines in Table 2 fail to learn the entire Pareto front and struggle with high data heterogeneity. Their performance deteriorates as heterogeneity increases. HetPFL not only learns the entire Pareto front but also handles high heterogeneity effectively; (II) **Scalability:** When compared with personalized FL methods such as EquiFL and PraFFL, our proposed HetPFL excels in handling high data heterogeneity in both



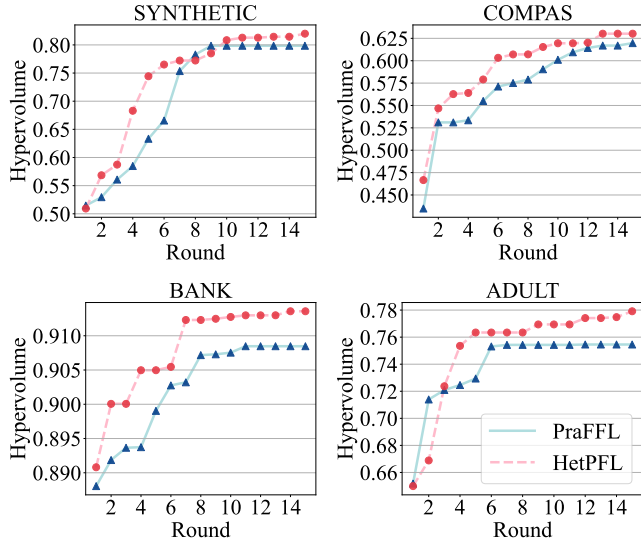


Figure 5: Convergence of HetPFL compared with PraFFL.

Table 2: Performance comparison across different heterogeneity levels on the SYNTHETIC dataset. The smaller the heterogeneity parameter, the greater the data heterogeneity.

Method	Local HV			Global HV		
	Heterogeneity Param.			Heterogeneity Param.		
	0.1	5	1000	0.1	5	1000
LFT+Ensemble	0.311	0.481	0.463	0.487	0.487	0.475
LFT+Fedavg	0.593	0.692	0.701	0.468	0.468	0.468
Agnosticfair	0.417	0.535	0.526	0.537	0.537	0.537
FairFed	0.392	0.349	0.410	0.429	0.400	0.403
FedFB	0.518	0.602	0.597	0.616	0.615	0.607
EquiFL	0.734	0.626	0.615	0.584	0.644	0.643
PraFFL	<u>0.802</u>	<u>0.781</u>	<u>0.789</u>	<u>0.707</u>	<u>0.744</u>	<u>0.768</u>
HetPFL	<b>0.808</b>	<b>0.806</b>	<b>0.810</b>	<b>0.820</b>	<b>0.791</b>	<b>0.817</b>

local and global datasets. EquiFL and PraFFL are better at handling high heterogeneity on local datasets, but they fail to address heterogeneity effectively on the global dataset.

**The Impact of the Number of Clients.** We analyze Table 3 from following two aspects: (I) **Comprehensiveness:** The first six methods in Table 3, which lack the capability to learn the Pareto front, exhibit limited performance in both small and large-scale client scenarios, with both local HV and global HV consistently below 0.7. In contrast, HetPFL not only learns the Pareto front but also achieves the best performance across all scenarios, with both local HV and global HV exceeding 0.78; (II) **Scalability:** Compared to PraFFL, HetPFL demonstrates clear advantages in large-scale client scenarios. Notably, PraFFL tends to collapse in learning the global Pareto front under large-scale settings, whereas HetPFL consistently achieves the best results in both local HV and global HV, regarding different client scales.

**Ablation Study.** Table 4 reveals two key observations: (I) PSA enhances the learning ability of the local Pareto front. On the SYNTHETIC dataset, the local HV improves from 0.80 to 0.83 with PSA. Similar improvements in local HV can

Table 3: Performance comparison of different methods across the number of clients on SYNTHETIC dataset.

Method	Local HV			Global HV		
	Number of Clients			Number of Clients		
	10	100	300	10	100	300
LFT+Ensemble	0.475	0.464	0.535	0.463	0.536	0.470
LFT+Fedavg	0.664	0.472	0.605	0.460	0.589	0.469
Agnosticfair	0.548	0.557	0.547	0.551	0.635	0.553
FairFed	0.414	0.326	0.413	0.372	0.381	0.353
FedFB	0.610	0.599	0.562	0.613	<u>0.667</u>	0.581
EquiFL	0.564	0.602	0.620	0.613	0.573	0.607
PraFFL	<u>0.803</u>	<u>0.716</u>	<u>0.789</u>	<u>0.807</u>	0.578	<u>0.621</u>
HetPFL	<b>0.808</b>	<b>0.785</b>	<b>0.848</b>	<b>0.808</b>	<b>0.814</b>	<b>0.813</b>

Table 4: Ablation experiments on preference sampling adaptation (PSA) and preference-aware hypernet fusion (PHF).

Dataset	PSA	PHF	Local HV	Global HV
SYNTHETIC	×	×	0.800	0.719
	×	✓	0.800	0.793
	✓	×	0.830	0.825
	✓	✓	<b>0.830</b>	<b>0.827</b>
COMPAS	×	×	0.599	0.613
	×	✓	0.599	<b>0.639</b>
	✓	×	0.623	0.624
	✓	✓	<b>0.623</b>	0.626
BANK	×	×	0.901	0.895
	×	✓	0.901	0.896
	✓	×	0.904	0.886
	✓	✓	<b>0.904</b>	<b>0.898</b>
ADULT	×	×	0.766	0.750
	×	✓	0.766	0.846
	✓	×	0.783	0.813
	✓	✓	<b>0.783</b>	<b>0.846</b>

be observed across the other three datasets. (II) PHF enhances the performance of the global Pareto front. Without PSA, PHF achieves an approximately 8% improvement in global HV on the SYNTHETIC dataset (from 0.719 to 0.793). With PSA, the improvement is smaller (i.e., 0.2%) due to the high global HV had been achieved by PSA (i.e., 0.825). Similar patterns can be observed on the other three datasets.

## 5 Conclusion

In this paper, we proposed HetPFL, a comprehensive method for learning both local and global Pareto fronts in fair federated learning. First, HetPFL includes a Preference Sampling Adaptation (PSA) approach, which adaptively learns the preference sampling distribution for each client. Second, HetPFL incorporates a Preference-aware Hypernet Fusion (PHF) approach, which guides the generation of the global hypernet by learning the mapping from preferences to fusion weights at the server. We prove that HetPFL achieves an error convergence rate of order  $\mathcal{O}(\frac{1}{t})$ . Experimental results show that HetPFL outperforms seven state-of-the-art methods in learning both local and global Pareto fronts across four datasets.

## Acknowledgments

This work was supported in part by the National Natural Science Foundation of China under Grant 62202214 and Guangdong Basic and Applied Basic Research Foundation under Grant 2023A1515012819.

## References

- [Barenstein, 2019] Matias Barenstein. Propublica’s compas data revisited. *arXiv preprint arXiv:1906.04711*, 2019.
- [Collins et al., 2021] Liam Collins, Hamed Hassani, Aryan Mokhtari, and Sanjay Shakkottai. Exploiting shared representations for personalized federated learning. In *Proceedings of International Conference on Machine Learning*, pages 2089–2099. PMLR, 2021.
- [Deng et al., 2020] Yuyang Deng, Mohammad Mahdi Kamani, and Mehrdad Mahdavi. Distributionally robust federated averaging. In *Proceedings of Advances in Neural Information Processing Systems*, volume 33, pages 15111–15122, 2020.
- [Du et al., 2021] Wei Du, Depeng Xu, Xintao Wu, and Hanghang Tong. Fairness-aware agnostic federated learning. In *Proceedings of the 2021 SIAM International Conference on Data Mining (SDM)*, pages 181–189. SIAM, 2021.
- [Dua et al., 2017] Dheeru Dua, Casey Graff, et al. Uci machine learning repository, 2017. URL <http://archive.ics.uci.edu/ml>, 7(1):62, 2017.
- [Ezzeldin et al., 2023] Yahya H Ezzeldin, Shen Yan, Chaoyang He, Emilio Ferrara, and A Salman Avestimehr. Fairfed: Enabling group fairness in federated learning. In *Proceedings of the AAAI Conference on Artificial Intelligence*, volume 37, pages 7494–7502, 2023.
- [Feldman et al., 2015] Michael Feldman, Sorelle A Friedler, John Moeller, Carlos Scheidegger, and Suresh Venkatasubramanian. Certifying and removing disparate impact. In *proceedings of the 21th ACM SIGKDD international conference on knowledge discovery and data mining*, pages 259–268, 2015.
- [Hong et al., 2023] Mingyi Hong, Hoi-To Wai, Zhaoran Wang, and Zhuoran Yang. A two-timescale stochastic algorithm framework for bilevel optimization: Complexity analysis and application to actor-critic. *SIAM Journal on Optimization*, 33(1):147–180, 2023.
- [Imteaj and Amini, 2022] Ahmed Imteaj and M Hadi Amini. Leveraging asynchronous federated learning to predict customers financial distress. *Intelligent Systems with Applications*, 14:200064, 2022.
- [Kamishima et al., 2012] Toshihiro Kamishima, Shotaro Akaho, Hideki Asoh, and Jun Sakuma. Fairness-aware classifier with prejudice remover regularizer. In *Machine Learning and Knowledge Discovery in Databases: European Conference, ECML PKDD 2012, Bristol, UK, September 24-28, 2012. Proceedings, Part II 23*, pages 35–50. Springer, 2012.
- [Li et al., 2019] Tian Li, Maziar Sanjabi, Ahmad Beirami, and Virginia Smith. Fair resource allocation in federated learning. *arXiv preprint arXiv:1905.10497*, 2019.
- [Lin et al., 2022] Xi Lin, Zhiyuan Yang, and Qingfu Zhang. Pareto set learning for neural multi-objective combinatorial optimization. In *Proceedings of International Conference on Learning Representations*, 2022.
- [Lyu et al., 2020] Lingjuan Lyu, Xinyi Xu, Qian Wang, and Han Yu. Collaborative fairness in federated learning. *Federated Learning: Privacy and Incentive*, pages 189–204, 2020.
- [Makhija et al., 2024] Disha Makhija, Xing Han, Joydeep Ghosh, and Yejin Kim. Achieving fairness across local and global models in federated learning. *arXiv preprint arXiv:2406.17102*, 2024.
- [McMahan et al., 2017] Brendan McMahan, Eider Moore, Daniel Ramage, Seth Hampson, and Blaise Aguera y Arcas. Communication-efficient learning of deep networks from decentralized data. In *Artificial Intelligence and Statistics*, pages 1273–1282. PMLR, 2017.
- [Miettinen, 1999] Kaisa Miettinen. *Nonlinear multiobjective optimization*, volume 12. Springer Science & Business Media, 1999.
- [Moro et al., 2014] Sérgio Moro, Paulo Cortez, and Paulo Rita. A data-driven approach to predict the success of bank telemarketing. *Decision Support Systems*, 62:22–31, 2014.
- [Nguyen et al., 2021] Dinh C Nguyen, Ming Ding, Pubudu N Pathirana, Aruna Seneviratne, Jun Li, and H Vincent Poor. Federated learning for internet of things: A comprehensive survey. *IEEE Communications Surveys & Tutorials*, 23(3):1622–1658, 2021.
- [Rieke et al., 2020] Nicola Rieke, Jonny Hancox, Wenqi Li, Fausto Milletari, Holger R Roth, Shadi Albarqouni, Spyridon Bakas, Mathieu N Galtier, Bennett A Landman, Klaus Maier-Hein, et al. The future of digital health with federated learning. *NPJ digital medicine*, 3(1):1–7, 2020.
- [Roh et al., 2020] Yuji Roh, Kangwook Lee, Steven Euijong Whang, and Changho Suh. Fairbatch: Batch selection for model fairness. *arXiv preprint arXiv:2012.01696*, 2020.
- [Salazar et al., 2023] Teresa Salazar, Miguel Fernandes, Helder Araújo, and Pedro Henriques Abreu. Fair-fate: Fair federated learning with momentum. In *Proceedings of International Conference on Computational Science*, pages 524–538. Springer, 2023.
- [Salimans et al., 2017] Tim Salimans, Jonathan Ho, Xi Chen, Szymon Sidor, and Ilya Sutskever. Evolution strategies as a scalable alternative to reinforcement learning. *arXiv preprint arXiv:1703.03864*, 2017.
- [Thapa et al., 2022] Chandra Thapa, Pathum Chamikara Mahawaga Arachchige, Seyit Camtepe, and Lichao Sun. Splitfed: When federated learning meets split learning. In *Proceedings of the AAAI Conference on Artificial Intelligence*, volume 36, pages 8485–8493, 2022.



- [Wang *et al.*, 2021] Zheng Wang, Xiaoliang Fan, Jianzhong Qi, Chenglu Wen, Cheng Wang, and Rongshan Yu. Federated learning with fair averaging. *arXiv preprint arXiv:2104.14937*, 2021.
- [Ye *et al.*, 2025] Rongguang Ye, Wei-Bin Kou, and Ming Tang. Praffl: A preference-aware scheme in fair federated learning. In *Proceedings of the 31st ACM SIGKDD Conference on Knowledge Discovery and Data Mining V.1*, page 1797–1808, 2025.
- [Yue *et al.*, 2023] Xubo Yue, Maher Nouiehed, and Raed Al Kontar. Gifair-fl: A framework for group and individual fairness in federated learning. *INFORMS Journal on Data Science*, 2(1):10–23, 2023.
- [Zeng *et al.*, 2021] Yuchen Zeng, Hongxu Chen, and Kangwook Lee. Improving fairness via federated learning. *arXiv preprint arXiv:2110.15545*, 2021.
- [Zeng *et al.*, 2023] Yuchen Zeng, Hongxu Chen, and Kangwook Lee. Federated learning with local fairness constraints. In *Proceedings of IEEE International Symposium on Information Theory (ISIT)*, pages 1937–1942. IEEE, 2023.
- [Zitzler and Thiele, 1999] Eckart Zitzler and Lothar Thiele. Multiobjective evolutionary algorithms: a comparative case study and the strength pareto approach. *IEEE transactions on Evolutionary Computation*, 3(4):257–271, 1999.

## A Schematic diagram

Fig. 6 shows the concept of Pareto front, Pareto optimal solution and weakly Pareto optimal solution in the problem of minimizing two objectives. The green dots correspond to the Pareto optimal solutions, i.e., the optimal solution, under one trade-off. The green line corresponds to the Pareto front, which is the optimal solution under all trade-offs. The orange dots are weakly Pareto optimal solutions, which achieve the optimality in one objective while cannot guarantee the quality of the other objective.

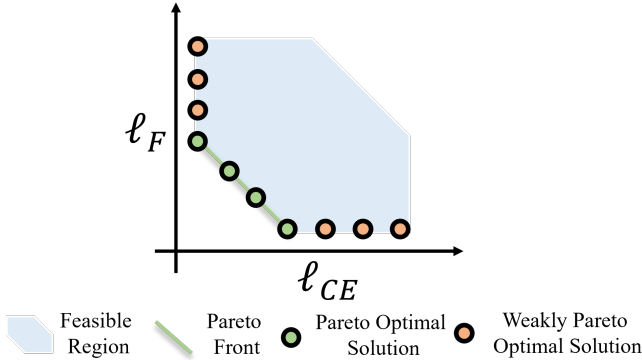


Figure 6: Schematic diagram of Pareto optimal solution, weakly Pareto optimal solution, and Pareto front.

## B Proof of Theorem 1

The proof logic proceeds as follows: Firstly, we give the upper bounds of the hypernet and the optimized sampling distribution within each iteration of a round (Lemma 3). Next, we prove the convergence relationship between the hypernet and the communicated model at round  $t$ . Finally, since the hypernet and the optimization of sampling distribution are coupled, we further consider the influence of the sampling distribution to derive the upper bound of the hypernet at any given round  $t$ .

Before proving Theorem 1, we give the upper bounds of the hypernet and the optimized sampling distribution within each iteration of a round as follows:

**Lemma 3** (Convergence of the Hypernet and Sampling Distribution in One Round [Hong *et al.*, 2023]). *If hypernet's learning rate  $\eta_h$  and sampling distribution's learning rate  $\kappa_s$  for any local iterations  $s > 0$  satisfy*

$$\begin{aligned} \kappa_s &\leq \min\{c_1 \eta^{\frac{3}{2}}, \frac{1}{\mu_2}\}, \frac{\eta_{s-1}}{\eta_s} \leq 1 + \frac{\eta_s \mu_1}{8}, \frac{\kappa_{s-1}}{\kappa_s} \leq 1 + \frac{3\kappa_s \mu_2}{4}, \\ \eta_s &\leq \min\{c_2 \kappa_s^{\frac{2}{3}}, \frac{1}{\mu_1}, \frac{\mu_1}{L_{t1}^2 \sigma_1^2}, \frac{\mu_1^2}{48c_1^2 L^2 L_q^2}\}, 8\mu_2 \kappa_s \leq \mu_1 \eta_s, \forall s \geq 0, \\ \text{where } c_1 > 0, c_2 > 0, L &= L_{h1} + \frac{L_{t4} G_1}{\mu_1} + G_2 \left( \frac{L_{t2}}{\mu_1} + \frac{L_{h3} G_1}{\mu_1^2} \right), \\ L_q \text{ are constants, then we have} \end{aligned}$$

$$\begin{aligned} \Delta_{\alpha_k}^s &\leq \left[ \prod_{j=0}^{s-1} (1 - \kappa_j \mu_2) \right] \left[ \Delta_{\alpha_k}^0 + \frac{L^2}{\mu_2^2} \Delta_{\beta_k}^0 \right] \\ &\quad + \frac{c_2 L^2}{\mu_2^2} \left[ \frac{\sigma_1^2}{\mu_1} + \frac{c_1^2 L_{q1}^2}{\mu_1} \sigma_3^2 \right] (\kappa_{s-1})^{\frac{2}{3}} + \frac{b_q^2}{\mu_2^2}, \end{aligned} \quad (19)$$

## Algorithm 1 HetPFL algorithm

---

```

1: Input:  $K, \mathcal{D}_{k \in [K]}, T, \tau_c, \tau_p, \eta_t, \eta_u, \eta_h, \kappa_h, N, U, \tilde{\lambda}$ 
2: Output:  $\{\psi_k\}_{k \in [K]}, \{\beta_k\}_{k \in [K]}, \psi$ , and  $\varphi$ 
3: // Each client initializes a hypernetwork  $\beta_k$ 
4: for  $t = 1$  to  $T$  do
5:   // Server sends aggregated model  $\psi_k$  to clients
6:   for client  $k \in [K]$  in parallel do
7:     // Optimize the communicated model
8:     for  $s = 1$  to  $\tau_c$  do
9:       Update  $\psi_k$  by Eq. (11);
10:    end for
11:   // Optimize the hypernet and sampling distribution
12:   for  $h = 1$  to  $\tau_p$  do
13:     Sample the preference vector  $\lambda \in p(\alpha_k)$ ;
14:     Update  $\beta_k$  by Eq. (12);
15:     Update  $\alpha_k$  by Eq. (14);
16:   end for
17: end for
18: // Server aggregates the communicated model
19:  $\psi = \frac{1}{K} \sum_{k=1}^K \psi_k$ ;
20: end for
21: // Optimize the FusionNet  $\varphi$ 
22: for  $u = 1$  to  $U$  do
23:   Update  $\varphi$  by Eq. (16);
24: end for
25: Return:  $\{\psi_k\}_{k \in [K]}, \{\beta_k\}_{k \in [K]}, \psi$ , and  $\varphi$ 

```

---

$$\Delta_{\beta_k}^s \leq \left[ \prod_{j=0}^{s-1} \left( 1 - \frac{\eta_j \mu_1}{4} \right) \right] \Delta_{\beta_k}^0 + \left[ \frac{\sigma_1^2}{\mu_1} + \frac{c_1^2 L_{q1}^2}{\mu_1^2} \right] \eta_{s-1}, \quad (20)$$

where  $\sigma_1, \sigma_2$ , and  $\sigma_3$  are constants.

We further analyze the convergence relationship between the hypernet and the communicated model across different rounds. Among them, we incorporate the impact of Eqs. (19) and (20) on the convergence of hypernet  $\mathbb{E} [\|\beta_k^{t+1} - \beta_k^*\|^2]$  at round  $t + 1$ .

$$\begin{aligned} &\mathbb{E} [\|\beta_k^{t+1} - \beta_k^*\|^2] \\ &= \mathbb{E} [\|\beta_k^t - \eta_t \nabla_{\beta} g(\beta_k^t, \psi^t) - \beta_k^*\|^2] \end{aligned} \quad (21)$$

$$\begin{aligned} &= \mathbb{E} [\|\beta_k^t - \beta_k^*\|^2] + \eta_t^2 \mathbb{E} [\|I_k^t \nabla_{\beta} g(\beta_k^t, \psi^t)\|^2] \\ &\quad + 2\eta_t \mathbb{E} [p_k \nabla_{\beta} g(\beta_k^t, \psi^t)^T (\beta_k^* - \beta_k^t)] \end{aligned} \quad (22)$$

$$\begin{aligned} &\stackrel{(a)}{\leq} (1 - \eta_t L_{t1}) \mathbb{E} [\|\beta_k^t - \beta_k^*\|^2] + \underbrace{\eta_t^2 \mathbb{E} [\|\nabla_{\beta} g(\beta_k^t; \psi^t)\|^2]}_{C_1} \\ &\quad + \underbrace{2\eta_t \mathbb{E} [g(\beta_k^*, \psi^t) - g(\beta_k^t, \psi^t)]}_{C_2}, \end{aligned} \quad (23)$$

where (a) is due to the smoothness of  $g$ . We then find the upper bounds of  $C_1$  and  $C_2$ , respectively. For  $C_1$ ,

$$\begin{aligned}
& \eta_t^2 \mathbb{E} [\|\nabla_{\beta} g(\beta_k^t, \psi^t)\|^2] \\
&= \eta_t^2 \mathbb{E} [\|\nabla_{\beta} g(\beta_k^t, \psi^t) - \nabla_{\beta} g(\beta_k^t, \psi^*) + \nabla_{\beta} g(\beta_k^t, \psi^*)\|^2] \quad (24) \\
&= 2\eta_t^2 \mathbb{E} [\|\nabla_{\beta} g(\beta_k^t, \psi^*)\| \|\nabla_{\beta} g(\beta_k^t, \psi^t) - \nabla_{\beta} g(\beta_k^t, \psi^*)\|] \\
&\quad + \eta_t^2 \mathbb{E} [\|\nabla_{\beta} g(\beta_k^t, \psi^*)\|^2] \\
&\quad + \eta_t^2 \mathbb{E} [\|\nabla_{\beta} g(\beta_k^t, \psi^t) - \nabla_{\beta} g(\beta_k^t, \psi^*)\|^2] \quad (25) \\
&\stackrel{(b)}{\leq} \eta_t^2 \mathbb{E} [\|\nabla_{\beta} g(\beta_k^t, \psi^*)\|^2] \\
&\quad + 2\eta_t^2 L_{t1} \mathbb{E} [\|\nabla_{\beta} g(\beta_k^t, \psi^*)\| \|\psi^t - \psi^*\|] \\
&\quad + \eta_t^2 \tilde{L}^2 \mathbb{E} [\|\psi^t - \psi^*\|^2], \quad (26)
\end{aligned}$$

where (b) is due to the convexity of  $g$ . Then, we continue to find the upper bound of  $C_2$ ,

$$\begin{aligned}
& 2\eta_t \mathbb{E} [g(\beta_k^*, \psi^t) - g(\beta_k^t, \psi^t)] \\
&\stackrel{(c)}{\leq} 2\eta_t \mathbb{E} [g(\beta_k^*, \psi^t) - g(\beta_k^t, \psi^t)] \\
&\quad + \eta_t (L_{t1} - \mu_1) \|\psi^t - \psi^*\|^2 \\
&\quad + \mathbb{E} [(\nabla_{\beta} g(\beta_k^*, \psi^t) - \nabla_{\beta} g(\beta_k^t, \psi^t))^T (\psi^t - \psi^*)] \\
&\stackrel{(d)}{\leq} 2\eta_t \mathbb{E} [g(\beta_k^*, \psi^t) - g(\beta_k^t, \psi^t)] \\
&\quad + \eta_t (L_{t1} - \mu_1) \|\psi^t - \psi^*\|^2 \\
&\quad + 2\eta_t L_{t1} \mathbb{E} [\|\phi_k^t - \phi_k^*\| \|\psi_k^t - \psi_k^*\|], \quad (27)
\end{aligned}$$

where (c) uses the smoothness and convexity of  $g$ . (d) uses the convexity of  $g$ . So far, we have found the upper bounds of  $C_1$  and  $C_2$ . We then plugging their upper bounds Eq. (26) and Eq. (27) into Eq. (23), as follows:

$$\begin{aligned}
& \mathbb{E} [\|\beta_k^{t+1} - \beta_k^*\|^2] \\
&\leq (1 - \eta_t \mu_1) \mathbb{E} [\|\beta_k^t - \beta_k^*\|^2] + \eta_t^2 \mathbb{E} [\|\nabla_{\beta} g(\beta_k^t, \psi^*)\|^2] \\
&\quad + 2\eta_t^2 L_{t1} \mathbb{E} [\|\nabla_{\beta} g(\beta_k^t, \psi^*)\| \|\psi^t - \psi^*\|] \\
&\quad + \eta_t^2 L_{t1}^2 \mathbb{E} [\|\psi^t - \psi^*\|^2] + 2\eta_t \mathbb{E} [g(\beta_k^*, \psi^t) - g(\beta_k^t, \psi^t)] \\
&\quad + 2\eta_t L_{t1} \mathbb{E} [\|\beta_k^t - \beta_k^*\| \|\psi^t - \psi^*\|] \\
&\quad + \eta_t (L_{t1} - \mu_1) \mathbb{E} [\|\psi^t - \psi^*\|^2] \quad (28) \\
&\stackrel{(e)}{\leq} (1 - \eta_t \mu_1) \mathbb{E} [\|\beta_k^t - \beta_k^*\|^2] + \eta_t^2 \mathbb{E} [\|\nabla_{\beta} g(\beta_k^t, \psi^*)\|^2] \\
&\quad + 2\eta_t^2 L_{t1} \sqrt{\mathbb{E} [\|\nabla_{\beta} g(\beta_k^t, \psi^*)\|^2] \mathbb{E} [\|\psi^t - \psi^*\|^2]} \\
&\quad + \eta_t^2 L_{t1}^2 \mathbb{E} [\|\psi^t - \psi^*\|^2] + \eta_t (L_{t1} - \mu_1) \mathbb{E} [\|\psi^t - \psi^*\|^2] \\
&\quad + 2\eta_t L_{t1} \sqrt{\mathbb{E} [\|\beta_k^t - \beta_k^*\|^2] \mathbb{E} [\|\psi^t - \psi^*\|^2]} \quad (29) \\
&\stackrel{(f)}{\leq} (1 - \eta_t \mu_1) \mathbb{E} [\|\beta_k^t - \beta_k^*\|^2] + 2\eta_t^2 G_3 L_{t1} \sqrt{\mathbb{E} [\|\psi^t - \psi^*\|^2]} \\
&\quad + \eta_t^2 G_3^2 + (\eta_t^2 L_{t1}^2 + \eta_t (L_{t1} - \mu_1)) \mathbb{E} [\|\psi^t - \psi^*\|^2] \\
&\quad + 2\eta_t L_{t1} \sqrt{\mathbb{E} [\|\beta_k^t - \beta_k^*\|^2] \mathbb{E} [\|\psi^t - \psi^*\|^2]}, \quad (30)
\end{aligned}$$

where (e) is due to the Cauchy-Schwarz inequality and  $\mathbb{E} [g(\beta_k^*, \psi^t) - g(\beta_k^t, \psi^t)] \leq 0$ . (f) holds because the norm of the squared gradient is bounded by  $G_3^2$ .

Eq. (30) describes the convergence relationship between the hypernet and the communicated model at each round. To further consider the impact of sampling distribution, we substitute Lemma 2 and Lemma 3 into the right side of the inequality Eq. (30). Then, we denote the convergence error of hypernet at round  $t+1$  as  $\Delta_{\beta_k}^{t+1} = \mathbb{E} [\|\beta_k^{t+1} - \beta_k^*\|^2]$ , its has the following upper bound:

$$\begin{aligned}
\Delta_{\beta_k}^{t+1} &\leq (1 - \mu_1 \eta_t) \left[ \left(\frac{3}{4}\right)^{\tau_p t} \Delta_{\beta_k}^0 + \left[ \frac{\sigma_1^2}{\mu_1^2} + \frac{c_1^2 L_{q1}^2}{\mu_1^3} \right] \right. \\
&\quad + 2\eta_t^2 G_3 L_{t1} (1 - \eta_t \zeta) \sqrt{\Delta_{\psi_k}^0} + \eta_t^2 G_3^2 \\
&\quad + (\eta_t^2 L_{t1}^2 + \eta_t (L_{t1} - \mu_1)) (1 - \eta_t \zeta)^{\frac{t}{2}} \Delta_{\psi_k}^0 \\
&\quad \left. + 2\eta_t L_{t1} (1 - \eta_t \zeta)^{\frac{t}{4}} \sqrt{\Delta_{\psi_k}^0} (\sqrt{\Delta_{\beta_k}^0} + \sqrt{\frac{\sigma_1^2}{\mu_1^2} + \frac{c_1^2 L_{q1}^2}{\mu_1^3}}) \right].
\end{aligned}$$

Let  $z_1 = 2\eta_t L_{t1} + \sqrt{\frac{\sigma_1^2 \mu_1 + c_1^2 L_{q1}^2}{\mu_1^3}}$  and  $z_2 = \eta_t^2 L_{t1}^2 + \eta_t (L_{t1} - \mu_1)$ . we get the following inequality:

$$\begin{aligned}
\Delta_{\beta_k}^{t+1} &\leq \left(\frac{3}{4}\right)^{\tau_p t} \Delta_{\beta_k}^0 + z_1 (1 - \eta_t \zeta)^{t/4} \sqrt{\Delta_{\psi_k}^0} \\
&\quad + z_2 (1 - \eta_t \zeta)^{t/2} \Delta_{\psi_k}^0 + \frac{\sigma_1^2 \mu_1 + c_1^2 L_{q1}^2 + G_3^2 \mu_1}{\mu_1^3} \\
&\quad + 2\eta_t L_{t1} (1 - \eta_t \zeta)^{t/4} \sqrt{\Delta_{\psi_k}^0 \Delta_{\beta_k}^0}. \quad (31)
\end{aligned}$$

## C Additional Experiments

### C.1 Experimental Details

#### Experimental Parameters

According to [Zeng *et al.*, 2021], we set the local epoch in each round to be 30 (i.e.,  $\tau_p + \tau_c = 30$ ). The total communication rounds  $T$  is set to 15, the batch size of data is 128 in the neural network training, and the batch size of sampling preference vectors  $N$  is 4. We use Adam as optimizer for communicated model, hypernet, and preference distribution optimization. The reference point  $r$  in calculating hypervolume is set to (1, 1). The preference sampling distribution  $p(\alpha_k)$ ,  $k \in [K]$ , is represented by Dirichlet distribution.

#### Dataset

According to the setting of [Zeng *et al.*, 2021; Ezzeldin *et al.*, 2023], the COMPAS and ADULT datasets have two clients, while the SYNTHETIC and BANK have three clients. This setting is common in cross-silo FL. In addition, we also conducted experiments with large-scale clients (e.g., 300 clients) in the experimental section.

The information of the four datasets is as follows:

- **SYNTHETIC** [Zeng *et al.*, 2021] is an artificially generated dataset containing 5000 samples with two non-sensitive features and a binary sensitive feature;
- **COMPAS** [Barenstein, 2019]: contains 7214 samples, 8 non-sensitive features, and 2 sensitive features (i.e., gender and race);
- **BANK** [Moro *et al.*, 2014] contains 45211 samples, 13 non-sensitive features, and one sensitive feature (i.e., age);

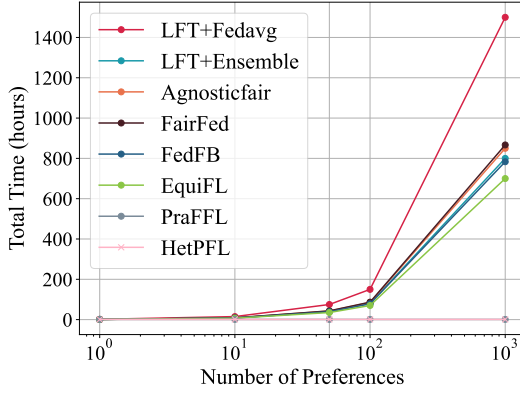


Figure 7: Comparison of the training time of the methods as the number of client preferences increases on the COMPAS dataset.

- **ADULT** [Dua *et al.*, 2017] contains 48842 samples, with 13 non-sensitive features and one sensitive feature (i.e., gender).

In the three real-world datasets, we split 30% of the data into the test set, and the other 70% of the data are split into the training set and validation set with a ratio of 9:1. Furthermore, we select the model that performs best in the validation set for testing.

### Baselines

The introduction of seven baselines is as follows:

- **LFT+Ensemble** learns fair classifiers from decentralized data without violating privacy policies by training locally fair classifiers and assembling them;
- **LFT+Fedavg** [Zeng *et al.*, 2023] applies FedAvg [McMahan *et al.*, 2017], under which the server periodically aggregates and synchronizes locally trained models;
- **Agnosticfair** [Du *et al.*, 2021] uses kernel reweighing functions to assign a reweighing value on each training sample in both loss function and fairness constraint;
- **FairFed** [Ezzeldin *et al.*, 2023] enhances group fairness via a fairness-aware aggregation method;
- **FedFB** [Zeng *et al.*, 2021] uses bi-level optimization to handle fairness. The lower layer is designed to optimize model performance and the upper layer is designed to improve model fairness;
- **EquiFL** [Makhija *et al.*, 2024] incorporates a fairness term and personalized layer into the local optimization, effectively balancing local performance and fairness;
- **PraFFL** [Ye *et al.*, 2025] design a method that can provide a preference-specific model in real time based on the client’s preferences, which has the ability to learn the entire Pareto front.

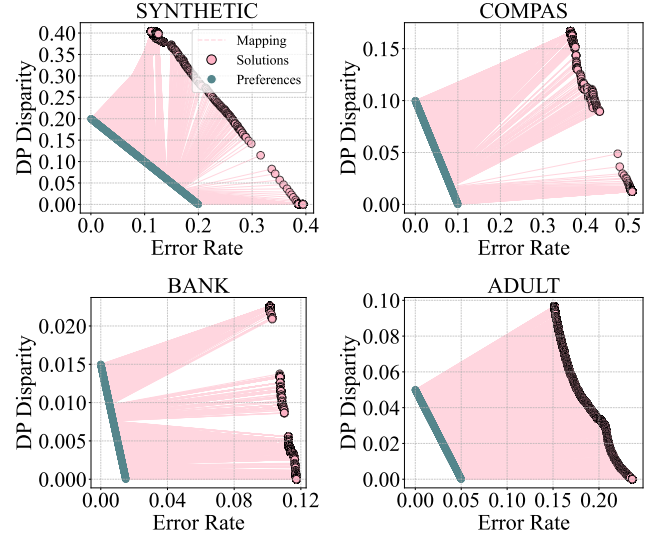


Figure 8: Visualization of HetPFL’s mapping from the preferred sampling space to the objective space on the global dataset.

### Neural Network Architecture.

The architecture of the communicated model  $\psi$  is as follow:

$$\begin{aligned} \psi(x) : x &\rightarrow \text{Linear}(|x|, 4) \rightarrow \text{ReLU} \\ &\rightarrow \text{Linear}(4, 4) \rightarrow \text{ReLU} \rightarrow x_{\text{mid}}, \end{aligned} \quad (32)$$

where  $x$  represent features of dataset.

The architecture of hypernet  $h_{\beta_k}$  is as follow:

$$\begin{aligned} h_{\beta_k} : \lambda &\rightarrow \text{Linear}(|\lambda|, 4) \rightarrow \text{ReLU} \\ &\rightarrow \text{Linear}(4, 4) \rightarrow \text{ReLU} \\ &\rightarrow \text{Linear}(4, |\phi_k|), \end{aligned} \quad (33)$$

where  $\lambda$  is preference vector, and the hypernetwork maps the preference vector to the personalized model  $\phi_k$ .

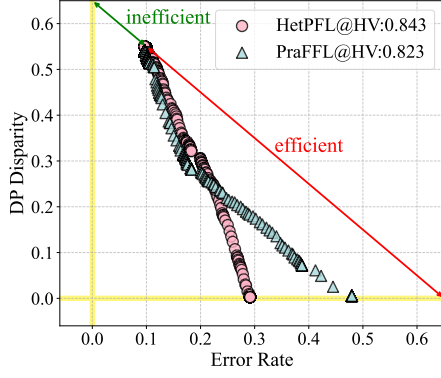
The architecture of FusionNet  $W_\varphi$  is as follows:

$$\begin{aligned} W_\varphi : \lambda &\rightarrow \text{Linear}(|\lambda|, 4) \rightarrow \text{ReLU} \\ &\rightarrow \text{Linear}(4, 4) \rightarrow \text{ReLU} \\ &\rightarrow \text{Linear}(4, K), \end{aligned} \quad (34)$$

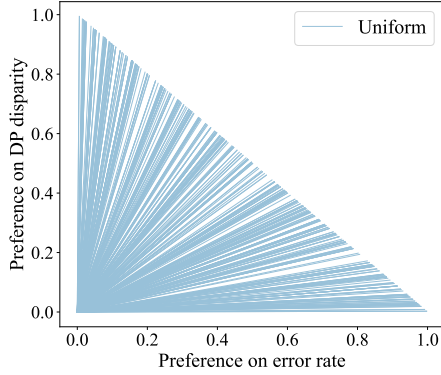
where  $K$  is the number of clients.

## C.2 Training Complexity under Different Preference Scales

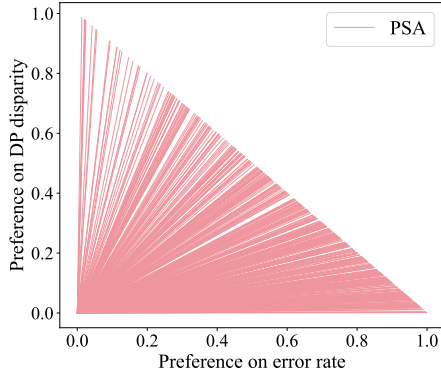
Fig. 7 illustrates the training complexity of different methods for large-scale preferences. For methods capable of learning the Pareto front like PraFFL and HetPFL, they have learned the mapping from client preferences to corresponding models during the training phase. As a result, during the inference phase, they only need to substitute client’s preferences to generate corresponding preference-specific models. Therefore, their time complexity is  $O(1)$ . In contrast, for methods that cannot learn the Pareto front, their training complexity increases linearly with the number of client preferences.



(a) The local Pareto front learned by a client on the SYNTHETIC.



(b) PraFFL's preference sampling distribution.



(c) HetPFL's preference sampling distribution.

Figure 9: Comparison of Preference Sampling Distributions.

### C.3 Visualization of Mapping

Fig. 8 shows the mapping results of 1000 preference vectors by HetPFL across four datasets. To enhance visual clarity, we scale the preference sampling space. Each pink line represents a mapping from a preference to its corresponding model's performance and fairness. It can be observed that HetPFL can map preference vectors to the Pareto front. Notably, on the ADULT dataset, HetPFL achieves particularly favorable results, as the mapping from preference vectors to the Pareto front is quite dense. On the SYNTHETIC dataset, some intersecting mapping paths appear mainly because dur-

ing the optimization phase, the objective is formulated using loss functions, which differs from the error rate and DP disparity presented in the figure.

### C.4 Visualization of Preference Sampling Distribution

Fig. 9 shows the Pareto fronts on a client and sampling distributions learned by PraFFL and HetPFL on the client using the SYNTHETIC dataset. We observe that the preference vector pointing to the green arrow area has no intersection with the Pareto front, while the preference vector pointing to the red arrow area has an intersection with the Pareto front. According to Proposition 1, sampling preferences from the green area is inefficient for learning the Pareto front. Instead, an effective preference sampling distribution should focus more on the directions where the Pareto front is located (i.e., red area). Fig. 9 (c) shows the sampling distribution of HetPFL. We can clearly observe that the density is higher on the direction of the Pareto front. Therefore, the sampling distribution learned by HetPFL is more advantageous than the uniform sampling distribution used by PraFFL (see Fig. 9 (b)).